ANL/RA/CP--80649
Conf-940407--15

To be Presented at the American Nuclear Society Topical Meeting on Advances in Reactor Physics, April 11-15, 1994, Knoxville, Tennessee

ANALYSIS OF EBR-II NEUTRON AND PHOTON PHYSICS BY MULTIDIMENSIONAL TRANSPORT-THEORY TECHNIQUES*

R. P. Jacqmin[a]
G. Palmiotti[b]
P. J. Finck[c]

[a]Argonne National Laboratory
Reactor Analysis Division
Argonne, IL 60439 U.S.A.

[b]CEA/CE Cadarache, SPRC BAT. 230
13108 Saint-Paul-les-Durance, France
Present address: Argonne National Laboratory
Reactor Analysis Division
Argonne, IL 60439 U.S.A.

[c]Argonne National Laboratory
Reactor Analysis Division
Argonne, IL 60439 U.S.A.
Present address: CEA/CE Cadarache, SPRC BAT. 230
13108 Saint-Paul-les-Durance, France

*Work supported by the U.S. Department of Energy, Nuclear Energy Programs under Contract W-31-109-ENG-38.

ANALYSIS OF EBR-II NEUTRON AND PHOTON PHYSICS BY MULTIDIMENSIONAL TRANSPORT-THEORY TECHNIQUES

R. P. Jacqmin[a]
G. Palmiotti[b]
P. J. Finck[c]

[a]Argonne National Laboratory, Reactor Analysis Division, Argonne, Illinois, 60439, USA
(708) 252-9283

[b]CEA/CE Cadarache, SPRC BAT. 230, 13108 Saint-Paul-les-Durance, France
Present address: Argonne National Laboratory, Reactor Analysis Division, Argonne, Illinois, 60439, USA

[c]Argonne National Laboratory, Reactor Analysis Division, Argonne, Illinois, 60439, USA
Present address: CEA/CE Cadarache, SPRC BAT. 230, 13108 Saint-Paul-les-Durance, France

ABSTRACT

This paper contains a review of the challenges specific to the EBR-II core physics, a description of the methods and techniques which have been developed for addressing these challenges, and the results of some validation studies relative to power-distribution calculations.

Numerical tests have shown that the VARIANT nodal code yields eigenvalue and power predictions as accurate as finite difference and discrete ordinates transport codes, at a small fraction of the cost. Comparisons with continuous-energy Monte Carlo results have proven that the errors introduced by the use of the diffusion-theory approximation in the collapsing procedure to obtain broad-group cross sections, kerma factors, and photon-production matrices, have a small impact on the EBR-II neutron/photon power distribution.

I. EBR-II PHYSICS CHALLENGES

Experimental Breeder Reactor II (EBR-II) is a small sodium-cooled fast reactor which is a key element of the demonstration of the Integral Fast Reactor fuel cycle closure. As that demonstration progresses, new challenges are being brought upon the methods and techniques used to calculate operational parameters.

The core of EBR-II is currently composed primarily of highly enriched U-10%Zr fuel. It has a small radius (R ~ 35 cm) and a pancake shape (H/D ~ 0.5). The radial configuration of EBR-II is particularly unique: the radial reflector is adjacent to the core and is surrounded by several rows of blanket subassemblies. The small size and unconventional configuration lead to a high neutron leakage fraction and important transport effects.

Accurate predictions of both neutron and photon power-distributions throughout EBR-II are required, not only in driver and blanket subassemblies, but also in low-power regions such as reflector or

structural subassemblies where photon heating dominates. During normal reactor operation, approximately 12% of the total power generated in EBR-II comes from photon heating. In driver subassemblies, photon heating amounts to only ~10% of total heating. However, in reflector and structural subassemblies, this fraction can be as high as 90%. In blanket subassemblies, it varies between 20 and 40% depending on subassembly location and irradiation history.

The standard procedure used at Argonne National Laboratory (ANL) to evaluate these power distributions consists of first performing a neutron flux-shape/eigenvalue calculation from a precomputed set of nine-group neutron interaction cross sections. Next, a photon source distribution is constructed as the product of group photon-production matrices and neutron flux. The photon flux is subsequently computed from this source and from a set of twenty-one-group photon interaction cross sections. Finally, neutron and photon power distributions are formed as the product of energy deposition (or "kerma") factors and fluxes. These distributions are normalized in amplitude to a specified total power level. The MC^2-2/SDX code package[1-2] is used to prepare assembly-homogenized broad-group microscopic cross sections, kerma factors, and photon-production matrices from intermediate-group (230 for neutrons, 94 for photons) libraries based on ENDF/B-V data.

The photon source and flux calculations would not be necessary if photon transport were negligible. Accurate total heating predictions could then be obtained directly from the neutron flux and the neutron energy-deposition factors augmented by the energy of the emitted photons. However, numerical tests have demonstrated that the transport of photons is significant in some EBR-II regions, and that the assumption of a local deposition of the photon energy leads to unacceptable errors in those regions. (Up to 50% overestimation in photon heating rate in the core, and up to 60% underestimation in the reflector.)

Because of the large fraction of neutrons leaking out of the core, the EBR-II reactor relies substantially on neutron reflection to maintain criticality. Recent work by Hill[3] has demonstrated that accurate predictions of certain key operational variables such as criticality and blanket powers require the use of three-dimensional (hexagonal-*Z*) transport codes and a large number of energy groups. Unfortunately, typical EBR-II models are very complex and employ large numbers of distinct compositions, making fine-mesh 3-*D* transport calculations prohibitively expensive.

However, some of these difficulties have been circumvented by the development of techniques to simplify core models, and by recent progress in coarse-mesh transport methods, in particular the development at ANL of the VARIANT nodal code.[4-5] A comprehensive effort aimed at validating this new code is under way. At the same time, and consistently with the anticipated improvements in flux shape calculations, numerical studies are being performed to assess the quality of the neutron and photon broad-group constants generated by the MC^2-2/SDX codes, and to identify possible areas were improvements may be needed. The results of some of these studies are described in this paper, following the presentation of numerical tests involving the VARIANT code.

II. VALIDATION OF VARIANT-COMPUTED EBR-II NEUTRON AND PHOTON POWER DISTRIBUTIONS

The theoretical basis of the VARIANT code is the Variational Nodal Method[4] in which the spatial and angular dependences of the even- and odd-parity group fluxes in each node are separated and expanded in terms of known basis functions (polynomials and spherical harmonics). A variational procedure is then applied to determine the coefficients of the expansions. This procedure results in a set of algebraic equations: (i) A neutron balance equation for each node; (ii) N continuity equations for the surface flux moments on each node interface, N being the order of the polynomial expansion of the even-parity flux within the nodes; and (iii) M continuity equations for the surface current moments on each node interface,

M being the order of the polynomial expansion of the odd-parity flux on the node surfaces. These equations are cast in conventional response matrix form and solved in standard iterative fashion.

The VARIANT code contains a diffusion option and a transport option. Recently, an anisotropic scattering capability was added.[5] The code can solve eigenvalue and fixed-source problems in Cartesian (2-D and 3-D), hexagonal, and hexagonal-Z geometries.

A 2-D, sixth-core, 154-node model of EBR-II was considered for a series of neutron/photon heating distribution calculations. VARIANT diffusion results were compared with DIF3D[6] finite difference results, while VARIANT transport results were compared with TWOHEX[7] S_{12} results. The same sets of cross sections, kerma factors, and photon-production matrices were used in all cases, and these group constants were assumed to be error-free. The VARIANT calculations used quadratic expansions on the node surfaces ($M = 2$), and sixth-order polynomial expansions in the interior of the nodes ($N = 6$).

Table 1 compares the total number of iterations and IBM RISC-6000 CPU times required by the different codes for computing the eigenvalue, k_{eff}, and the neutron flux distribution. Fixed-source photon flux calculations are compared in Table 2. DIF3D Nodal[8] results are also included in the tables for comparison purposes. A pointwise error reduction of 10^{-5} was required in all cases except in the DIF3D Nodal fixed-source calculation in which a fixed number of inner iterations was imposed.

Table 1. Compared Performance of the VARIANT, DIF3D, and TWOHEX Codes for EBR-II Nine-Group Neutron-Flux/Criticality Calculations.

	Outer Iters.	k_{eff}*	CPU Time (s) for all Outers	Overall CPU Time (s)
DIF3D Nodal	20	0.99597	0.72	0.72
VARIANT Diffusion	20	0.99566	2.6	3.5
DIF3D Finite Diff. (216 Triangles/Hex.)	17	0.99569	193.	215.
VARIANT Transport P_1	28	1.01404	25.	54.
TWOHEX $S_{12}P_1$ (54 Triangles/Hex.)	11	1.01424	8630.	8636.

*Reference k_{eff} = 0.99567, obtained with DIF3D, 600 triangles per hexagon.

Table 2. Compared Performance of the VARIANT, DIF3D, and TWOHEX Codes for EBR-II Twenty-One-Group Fixed-Source Photon Flux Calculations.

	Inner Iters.	CPU Time (s) for all Inners	Overall CPU Time (s)
DIF3D Nodal	10500	3.8	3.8
VARIANT Diffusion	4293	15.5	17.5
DIF3D Finite Diff. (216 Triangles/Hex.)	1671	42.8	91.4
VARIANT Transport P_3	5124	146.	208.

Table 2. Compared Performance of the VARIANT, DIF3D, and TWOHEX Codes for EBR-II Twenty-One-Group Fixed-Source Photon Flux Calculations.

	Inner Iters.	CPU Time (s) for all Inners	Overall CPU Time (s)
TWOHEX $S_{12}P_3$ (54 Triangles/Hex.)	166	3948.	3969.

The difference between the last two columns in the tables is the time required to compute the matrix coefficients. In the case of VARIANT, this time often amounts to a substantial fraction of the total CPU time for complex models.

The tables show that the VARIANT diffusion and transport options outperform the DIF3D finite difference and TWOHEX codes, respectively. The DIF3D Nodal diffusion code appears to be the fastest running, but the use of lower-order expansions (i.e., $M = 0$ and $N = 4$) would make the VARIANT running time comparable. Node-to-node comparisons of neutron and photon power distributions revealed that the VARIANT results agree very well with node-averaged fine-mesh results: maximum discrepancies in neutron heating are only 0.30% in the core, 0.31% radial reflector, and 0.59% blanket regions. The corresponding maximum errors in photon heating are 0.25%, -1.38%, and 0.47%, respectively. Note the fairly large difference (~2%) between the diffusion and transport eigenvalues.

These numerical tests illustrate the considerable potential of the VARIANT code for inexpensive yet accurate EBR-II criticality and power-distribution predictions.

III. ASSESSMENT OF THE NEUTRON BROAD-GROUP CONSTANTS

A. NEUTRON FLUX AND CROSS SECTIONS

As accurate and inexpensive flux calculations are becoming a reality, greater emphasis is being placed on the generation of improved sets of homogenized broad-group cross sections and kerma factors. Comparisons with continuous-energy Monte Carlo calculations[9] have shown that the methods currently in use for calculating nine-group neutron cross section sets are probably adequate for diffusion-theory based analyses of EBR-II. However, a number of difficulties associated with the generation of improved sets of broad group constants for more detailed EBR-II studies have been identified and reported by Hill.[3] In particular, Hill found that improved flux predictions in the reflector and blanket regions require that more than nine energy groups be retained. His results also suggested that the use of the diffusion-theory approximation, by the SDX code, for computing the various regional spectra for cross section condensation caused significant errors in the final broad-group constants. To get a more quantitative appreciation for the magnitude of the potential errors involved, detailed comparisons were performed between a two-dimensional 230-group DIF3D neutron flux calculation and a continuous-energy Monte Carlo MCNP[10] calculation.

An R-Z model of EBR-II was constructed specifically for these tests. This model is shown in Figure 1. It consists of 17 x 24 = 408 coarse meshes and 68 x 120 = 7160 fine meshes. The maximum fine-mesh dimensions are 1.34 cm by 1.51 cm. The subassemblies are assumed to be homogeneous. The core is composed of six rows of subassemblies containing metallic fuel (~65% U-235). The blanket is made of fresh subassemblies (0.05% Pu, depleted U). There are a total of 32 different material compositions, including 18 for the core region alone.

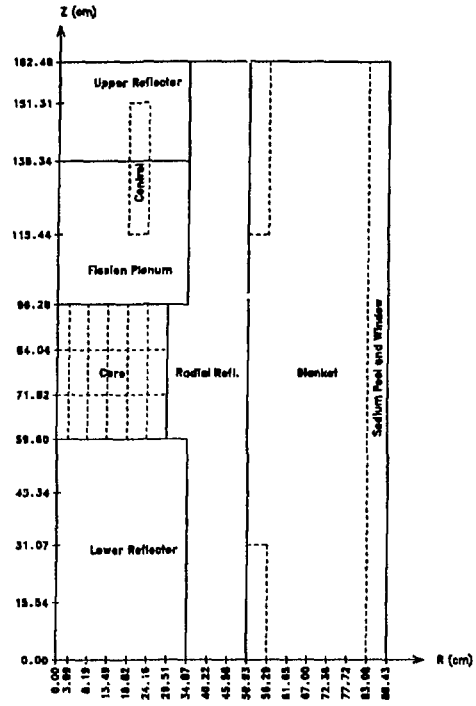

Fig. 1. *R-Z* Model of EBR-II Showing the Main Regions.

Libraries of 230 neutron and 94 photon group constants were generated from ENDF/B-V data at a uniform temperature of 300K for consistency with the MCNP libraries. The generation of these intermediate group constants was done with considerable care to obtain the "best possible" sets. Several additional simplifications were made in the model to allow consistent comparisons with MCNP. In particular:

- Fission products and some minor isotopes were eliminated;
- Delayed photons were excluded from the fission yields in the calculation of the photon production matrices; (They are normally included and account for ~25% of total photon power.)
- Delayed beta-ray energies were excluded from the neutron kerma factors. (They are normally present and account for ~3.5% of total neutron power.)

The MCNP code was run in a coupled neutron/photon mode so that information about both the neutron flux and the photon flux would be available. Broad-group flux and heating tallies were requested in all 408 coarse meshes. The neutron flux obtained from the fine-mesh, 230-group, DIF3D finite difference calculation averaged over each coarse mesh and condensed to nine broad groups. The resulting broad-group average fluxes were compared with the reference MCNP values (normalized to the same total fission source of 4.818×10^{18} neutrons/s).

The DIF3D-computed eigenvalue was 0.96981. This value is about 2% lower than the MCNP result of 0.9903 ± 0.0004, a rather large discrepancy caused by the cross section condensation and by the diffusion-theory approximation.

The maximum relative errors in the nine group fluxes are presented in Table 3 for EBR-II regions of

interest. The reflector and blanket regions considered in these comparisons extend three coarse meshes above and below the core. Comparisons were made not only with the average MCNP flux, ϕ_n^{MCNP}, but also with $\phi_n^{MCNP} - \sigma\left(\phi_n^{MCNP}\right)$ and with $\phi_n^{MCNP} + \sigma\left(\phi_n^{MCNP}\right)$ where $\sigma\left(\phi_n^{MCNP}\right)$ is the MCNP estimate of the standard deviation in ϕ_n^{MCNP}. The results of these two additional comparisons are indicated in Table 3 in the form of a $\pm 1\sigma$ uncertainty in the relative errors. The last column contains the MCNP-computed reactor-integrated flux in units of neutrons.cm.s^{-1}.

Table 3. Maximum Relative Errors (%) in Coarse-Mesh- and Broad-Group-Averaged DIF3D-Computed Neutron Flux.

Group (E_{top} in MeV)	Inner Core	Core	Radial Reflector Rows 7-8	Radial Reflector Rows 9-10	Blanket Rows 11-12	Blanket Rows 13-14	Control	Flux Integral (10^{18} cm s^{-1})
1 (14.2)	-9.10 ± 0.95	-12.8 ± 0.1	45.4 ± 3.3	-27.3 ± 4.5	-19.7 ± 5.4	22. ± 15.	24.2 ± 3.0	1.74 ± 0.03
2 (6.07)	-5.45 ± 0.15	-8.01 ± .18	24.3 ± 0.4	-18.5 ± 0.7	-15.2 ± 0.8	-9.1 ± 1.1	16.5 ± 0.4	69.1 ± 0.2
3 (1.35)	-4.37 ± 0.17	-5.48 ± 0.19	12.6 ± 0.2	11.2 ± 0.2	-9.65 ± 0.41	-12.4 ± 0.5	14.9 ± 0.3	165.4 ± 0.4
4 (0.498)	2.87 ± 0.16	4.89 ± 0.17	12.7 ± 0.2	12.8 ± 0.2	7.38 ± 0.22	-3.59 ± 0.33	17.1 ± 0.2	251.7 ± 0.5
5 (0.183)	-2.67 ± 0.40	5.24 ± 0.24	13.2 ± 0.2	12.5 ± 0.3	8.02 ± 0.22	7.35 ± 0.25	14.3 ± 0.3	213.7 ± 0.5
6 (0.0674)	4.29 ± 0.38	7.57 ± 0.37	11.4 ± 0.3	11.9 ± 0.3	10.5 ± 0.3	11.4 ± 0.3	11.5 ± 0.3	123.0 ± 0.4
7 (0.0248)	5.75 ± 0.70	6.97 ± 0.45	5.80 ± 0.32	5.89 ± 0.28	18.0 ± 0.4	20.7 ± 0.5	9.52 ± 0.30	96.1 ± 0.3
8 (0.00912)	9.1 ± 1.7	9.3 ± 1.5	9.34 ± 0.47	11.7 ± 0.6	40.8 ± 1.0	47.4 ± 1.0	8.38 ± 0.44	28.2 ± 0.2
9 (0.00335)	21.6 ± 1.6	28.0 ± 1.5	19.9 ± 0.5	23.2 ± 0.6	32.1 ± 0.7	53.8 ± 1.0	18.2 ± 0.5	91.0 ± 0.4

In the core, the magnitude of the errors does not exceed a few percent in the most important groups (Groups 2 through 7). Significantly larger discrepancies are observed in the other regions. In the reflector, fission plenum, and control regions, the neutron flux is overestimated in almost all meshes and all groups. In the radial reflector, at the core elevation (between z = 59.6 cm and z = 96.3 cm), this overestimation is generally in the 6% to 13% range, except in Group 7 where it is only about 4%, and in Group 9 where it is about 20%. In the blanket region, the DIF3D-computed neutron flux is too low at high energies (Groups 1-3), and too high at low energies (Groups 4-9). This is well illustrated by Figs. 2a and 2b which show plots of the relative errors in the Group 3 and Group 7 neutron fluxes along the mid-core radial traverse. The height of the error bars is equal to 2σ. In Groups 6 through 9, the overestimation is nearly uniform axially, with values ranging from ~10% in Group 6 to ~30% and more in Groups 8 and 9.

Such fairly large discrepancies in broad-group average fluxes are evidence that the 230-group DIF3D-computed neutron flux contains large errors. This confirms that significant improvements in the EBR-II neutron constants (in any broad-group structure) cannot be obtained with diffusion theory from the current intermediate-group structure. Only transport-theory calculations could possibly yield these desirable improvements.

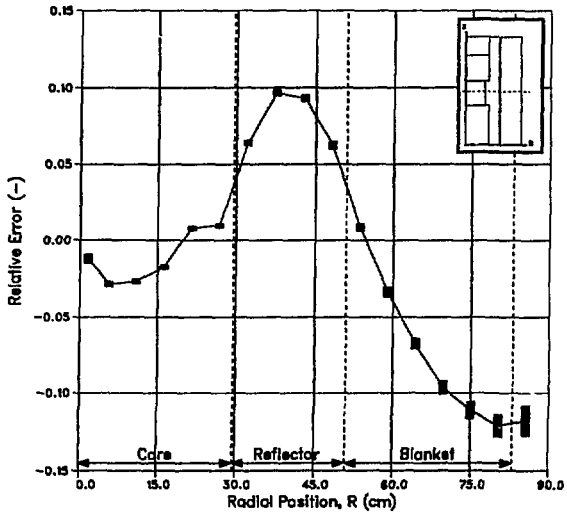

Fig. 2a. Relative Error in Group 3 Neutron Flux Versus *R* at Axial Coarse Mesh # 12.

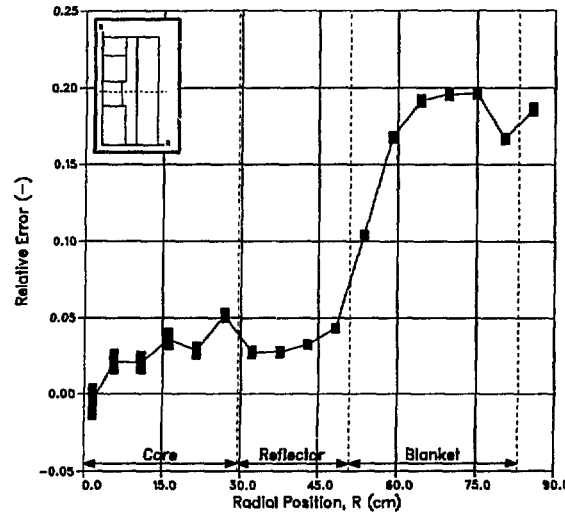

Fig. 2b. Relative Error in Group 7 Neutron Flux Versus *R* at Axial Coarse Mesh # 12.

B. NEUTRON KERMA FACTORS

Accurate predictions of the neutron power distribution in EBR-II require that reasonably good estimates not only of neutron group fluxes, but also of neutron group kerma factors be available. Isotopic kerma factors are computed as the product of the isotope total interaction cross section and the net average energy deposited locally as a result of all possible neutron-induced reactions.

To assess the quality of the standard set of nine-group kerma factors computed by the MC^2-2/SDX codes independently of errors in the neutron flux, a "hybrid" neutron heating distribution was formed as the group-integrated product of the kerma factors by the MCNP-computed neutron flux, ϕ_n^{MCNP}. This power distribution was then compared with the MCNP neutron heating tallies.

The maximum relative errors are presented in Table 4. To get an appreciation for the impact of statistical uncertainties in the MCNP flux, the comparisons were repeated with power distributions computed from $\phi_n^{MCNP} - \sigma\left(\phi_n^{MCNP}\right)$ and $\phi_n^{MCNP} + \sigma\left(\phi_n^{MCNP}\right)$, instead of ϕ_n^{MCNP}. The results of these additional comparisons are also included in Table 4.

Table 4. Maximum Relative Errors (%) in Coarse-Mesh Neutron Heating Computed as the Product of Neutron Kerma Factors by the MCNP Neutron Flux.

Neutron Flux	Inner Core	Core	Radial Reflector Rows 7-8	Radial Reflector Rows 9-10	Blanket Rows 11-12	Blanket Rows 13-14	Control	Total Neutron Power
ϕ_n^{MCNP}	0.51 ± 0.10	0.57 ± 0.10	13.8 ± 0.2	19.7 ± 0.2	-4.42 ± 0.39	-2.78 ± 0.67	54.4 ± 0.3	0.12 ± 0.12
$\phi_n^{MCNP} - \sigma\left(\phi_n^{MCNP}\right)$	-0.61 ± 0.10	0.83 ± 0.10	13.5 ± 0.2	19.4 ± 0.2	-5.06 ± 0.39	-3.81 ± 0.66	53.9 ± 0.3	-0.15 ± 0.12
$\phi_n^{MCNP} + \sigma\left(\phi_n^{MCNP}\right)$	0.77 ± 0.10	0.91 ± 0.19	14.2 ± 0.3	20.1 ± 0.2	-3.78 ± 0.39	-1.74 ± 0.67	54.9 ± 0.3	0.39 ± 0.12

Table 4 shows an excellent agreement in the core. Neutron power is overestimated in the reflector and control regions, while it is underestimated in the blanket region. Figures 3a and 3b show that the errors in the reflector and blanket regions actually increase in magnitude as one moves away from the axial midplane. However, these larger relative errors may be acccptable since they occur in lower-power regions. The very large overestimation in the control-rod region suggests that the boron kerma factors should be reevaluated. The 4.4% underestimation in the blanket occurs at a fairly low axial position. At the core level, neutron power in the blanket is underestimated by no more than 1.5%. (See Fig. 3b.) Note also that the computed total power agrees with to the MCNP result (51.980 ± 0.061 MW) to within statistical uncertainties.

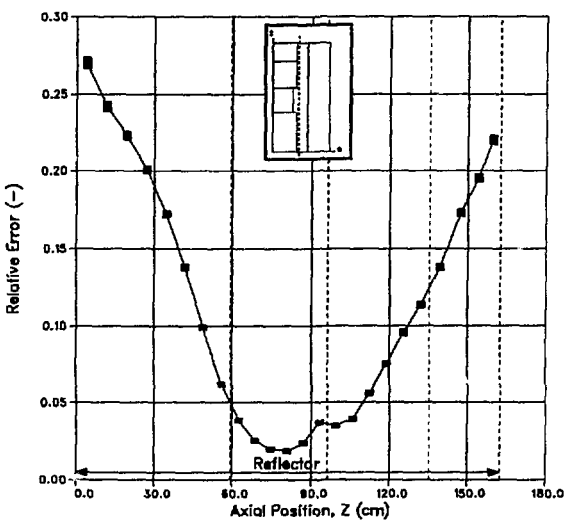

Fig. 3a. Relative Error in Neutron Heating Versus Z at Radial Coarse Mesh # 8 (Reflector).

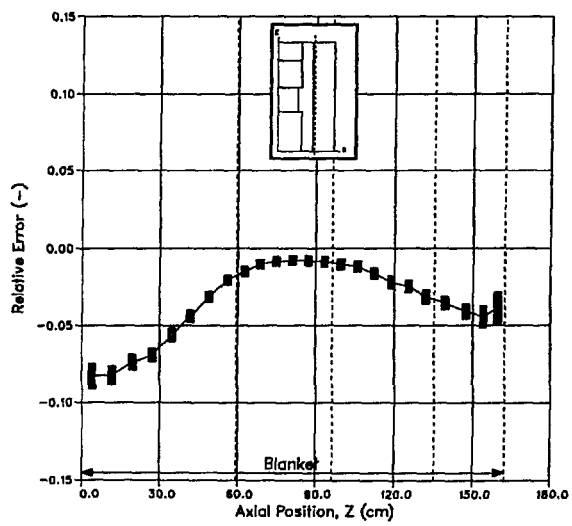

Fig. 3b. Relative Error in Neutron Heating Versus Z at Radial Coarse Mesh # 11 (Blanket).

From these comparisons, it can be concluded that the broad-group neutron kerma factors generated by the standard MC^2-2/SDX methodology are adequate in that, when combined with a good estimate of the

broad group neutron flux, they yield a fairly accurate neutron power distribution.

IV. ASSESSMENT OF THE PHOTON BROAD-GROUP CONSTANTS

Efforts have also been devoted to a careful validation of the libraries of 21-group *photon* interaction cross section and kerma factors generated by a special module in SDX. The foregoing *R-Z* model of EBR-II was also considered for this validation, but the reference results were obtained from a separate fixed-source MCNP calculation.

A 21-group, coarse-mesh, isotropic photon source distribution was precomputed and input to MCNP using standard MCNP source definition cards. This photon source was assumed to be error free. The position and energy of the source photons were sampled uniformly within each coarse mesh and group. The MCNP code was run in photon mode with the transport of fluorescent photons explicitly taken into account. To test the photon cross sections generated by SDX, a fine-mesh TWODANT[11] S_{16} P_3 photon-flux calculation, employing these cross sections, was carried out from the same photon source distribution. The quality of the photon group cross sections was evaluated by comparing the coarse-mesh averaged TWODANT-computed group fluxes with the MCNP results (normalized to the same total photon source level of 5.628×10^{19} photons/s).

These comparisons revealed relative errors of less than 5% in magnitude in nearly all coarse meshes, except in Groups 16 through 21 (i.e., below 150 KeV). In those low-energy groups, the photon flux in the core and blanket regions was underpredicted with TWODANT by more than 80%. The reason for these large discrepancies at low energies was identified as the neglect of the fluorescence reaction in the SDX-generated photon cross sections. The neglect of this photon-creation process is motivated by the fact that fluorescence photons are low-energy (< 122 KeV) photons that travel only very short distances compared with the EBR-II subassembly pitch, especially when materials with high atomic numbers are present. For such low-energy photons, a local energy deposition approximation should therefore give good results. The average energy normally carried away by the emitted fluorescence photons is included in the photon kerma factors as part of the photoelectric absorption process.

Table 5 shows the largest relative errors in coarse-mesh photon power density. The TWODANT-computed total photon power is 7.33 MW.

Table 5. Maximum Relative Errors (%) in Coarse-Mesh Photon Heating Rates Constructed From a High-Order Fixed-Source TWODANT Photon Flux Calculation.

Inner Core	Core	Radial Reflector Rows 7-8	Radial Reflector Rows 9-10	Blanket Rows 11-12	Blanket Rows 13-14	Control	Total Photon Power
-2.34±0.31	-2.34 ± 0.31	-1.84 ± 0.25	-1.05 ± 0.20	-2.19 ± 0.18	-2.18 ± 0.18	less than 1%	-1.24 ± 0.18

The errors appearing in Table 5 are all very small, which demonstrates that the TWODANT-computed photon heating distribution is in very good agreement with the MCNP results, despite a slight overall underestimation. This very good agreement is evidence that neglecting the transport of fluorescence photons in EBR-II is an excellent approximation. It is also evidence that the twenty-one-group structure, the photon interaction cross sections, and the photon kerma factors all are adequate for the purpose of obtaining accurate photon power predictions throughout the reactor.

V. ASSESSMENT OF THE PHOTON-PRODUCTION MATRICES

No matter how accurately the photon group constants are computed, photon heating will be poorly predicted if the photon source itself contains large errors. The quality of this photon-source distribution depends not only on the calculated neutron flux, but also on the precomputed set of broad-group photon-production matrices. Recall that the production mastrix for each nuclide is the sum over all photon-producing neutron-induced reactions of a neutron interaction cross section (for each neutron group n) multiplied by a photon yield (for each gamma group g).

The results of the coupled neutron/photon MCNP calculation were used to evaluate the quality of these photon-production matrices. First, a photon source was computed as the product of the photon-production matrices by the MCNP-computed neutron flux. Group-by-group comparisons of this photon source with the MCNP results was not possible because photon source tallies for individual photon groups were not available. It was therefore decided to compare instead the photon group fluxes obtained from this source by a fine-mesh, TWODANT S_{16} P_3 photon-flux calculation with the MCNP-computed photon group fluxes. The tests of the previous section have proved that, in the absence of errors in the photon source, such a TWODANT calculation yields an accurate photon flux in Groups 1 through 15. Therefore, if the photon flux comparisons reveal significant errors, these errors will have can be attributed to from the photon source, i.e., in this case, from the photon-production matrices. (Errors caused by the fact that the source distribution is not specified on a fine-mesh basis were studied independently and were shown to be small.)

The results of these group-to-group photon flux comparisons are presented in Table 6.

Table 6. Maximum Relative Errors (%) in Coarse-Mesh-Averaged Photon Flux Computed by the TWODANT Code From a Photon Source Formed as the Product of Photon-Production Matrices and MCNP-Computed Neutron Flux.

Group (E_{top} in MeV)	Inner Core	Core	Radial Reflector Rows 7-8	Radial Reflector Rows 9-10	Blanket Rows 11-12	Blanket Rows 13-14	Control	Flux Integral (10^{18} cm s^{-1})
2 (10.0)	10.3 ± 6.3	12.6 ± 6.5	-10.9 ± 0.8	-9.1 ± 0.7	-9.3 ± 2.5	-7.2 ± 1.9	-2.4 ± 1.4	1.11 ± 0.01
3 (8.0)	-13.6 ± 3.1	-17.6 ± 5.14	-27.9 ± 0.6	-25.9 ± 0.5	-22.6 ± 2.1	-24.1 ± 2.7	-24.0 ± 1.0	1.58 ± 0.02
4 (7.0)	12.9 ± 6.1	12.9 ± 6.1	-21.9 ± 0.9	-21.2 ± 0.9	-22.3 ± 3.1	-22.6 ± 2.6	-17.7 ± 1.7	0.74 ± 0.01
5 (6.0)	-5.9 ± 1.4	-8.0 ± 1.2	-22.6 ± 0.9	-19.8 ± 0.9	-19.8 ± 3.9	-21.1 ± 4.8	-12.2 ± 2.2	0.99 ± 0.02
6 (5.0)	-5.5 ± 2.5	-6.8 ± 2.9	-23.2 ± 0.9	-20.4 ± 0.9	-11.8 ± 0.8	-11.1 ± 1.0	-17.0 ± 1.8	1.71 ± 0.02
7 (4.0)	-5.5 ± 1.7	-5.5 ± 1.7	-18.6 ± 0.8	-21.4 ± 0.8	-11.2 ± 0.6	-9.51 ± 0.66	-6.0 ± 1.7	3.84 ± 0.04
8 (3.0)	-3.19 ± 0.59	-4.27 ± 0.59	-19.5 ± 1.0	-23.6 ± 0.8	-11.2 ± 0.5	-9.87 ± 0.57	-11.4 ± 2.0	3.90 ± 0.04
9 (2.5)	-3.2 ± 1.2	-3.2 ± 1.2	-16.7 ± 0.9	-24.7 ± 0.7	-11.0 ± 0.4	-9.82 ± 0.47	-10.5 ± 1.8	6.19 ± 0.04
10 (2.0)	-2.22 ± 0.37	-2.44 ± 0.37	-16.4 ± 0.8	-24.1 ± 0.6	-9.79 ± 0.33	-9.37 ± 0.33	-5.5 ± 1.5	10.04 ± 0.05
11 (1.5)	-1.48 ± 0.65	-2.82 ± 0.26	-8.52 ± 0.72	-17.9 ± 0.6	-8.83 ± 0.32	-8.30 ± 0.41	2.31 ± 0.92	17.30 ± 0.07
12 (1.0)	-2.08 ± 0.62	-2.73 ± 0.62	-5.03 ± 0.38	-10,3 ± 0.5	-8.23 ± 0.36	-7.77 ± 0.46	-2.21 ± 0.72	19.90 ± 0.07
13 (0.7)	-1.47 ± 0.24	-1.79 ± 0.22	-11.1 ± 0.4	-16.8 ± 0.4	-8.13 ± 0.27	-7.47 ± 0.34	68.1 ± 0.5	21.26 ± 0.07
14 (0.45)	-2.40 ± 0.26	-2.43 ± 0.24	-9.60 ± 0.4	-15.5 ± 0.4	-10.0 ± 0.4	-8.95 ± 0.45	20.9 ± 0.5	14.42 ± 0.05
15 (0.30)	-3.49 ± 0.23	-3.49 ± 0.23	-9.32 ± 0.37	-15.5 ± 0.3	-11.4 ± 0.3	-10.1 ± 0.4	37.4 ± 0.4	16.09 ± 0.05

Table 6 reveals maximum relative errors of only a few percent in the core in Groups 6 through 15. (These ten groups contribute approximately 95% of the photon heating in the core.) A detailed analysis shows that errors in regions immediately surrounding the core do not exceed 5% in magnitude in most groups. Larger discrepancies are observed farther away from the core. In the blanket, at the core elevation, the photon flux in all blanket rows is systematically underestimated by 7 to 10% in Groups 6 through 15. The anomalously large errors in Groups 13 through 15 in the control-rod region are most likely a consequence of poor B-10 photon-production values. (Recall that neutron capture in B-10 is followed by the emission of a 0.5 MeV gamma ray.)

These comparisons were repeated with the photon source formed from $\phi_n^{MCNP} - \sigma\left(\phi_n^{MCNP}\right)$ and $\phi_n^{MCNP} + \sigma\left(\phi_n^{MCNP}\right)$ instead of ϕ_n^{MCNP}. The results in either case were very similar to those obtained with ϕ_n^{MCNP}, thus providing evidence that statistical uncertainties in the neutron flux alone cannot explain the fairly large errors appearing in Table 6. Therefore, one can legitimately conclude that the approximations made in computing the broad-group photon-production matrices are the main cause of the errors observed. The rather poor blanket and reflector spectra used in collapsing the matrices are largely responsible for these errors.

The maximum relative errors in coarse-mesh photon heating are presented in Table 7.

Table 7. Maximum Relative Errors (%) in Photon Heating Computed by the TWODANT Code From a Photon Source Formed as the Product of Photon-Production Matrices by the MCNP-Computed Neutron Flux.

Neutron Flux	Inner Core	Core	Radial Reflector Rows 7-8	Radial Reflector Rows 9-10	Blanket Rows 11-12	Blanket Rows 13-14	Control	Total Photon Power
ϕ_n^{MCNP}	-1.24 ± 0.33	-2.20 ± 0.15	-16.5 ± 0.3	-17.3 ± 0.3	-9.28 ± 0.21	-7.98 ± 0.25	+21.6 ± 0.4	-4.17 ± 0.20
$\phi_n^{MCNP} - \sigma\left(\phi_n^{MCNP}\right)$	-1.60 ± 0.33	-2.47 ± 0.16	-16.8 ± 0.3	-17.6 ± 0.3	-9.61 ± 0.21	-8.41 ± 0.25	+22.1 ± 0.4	-4.47 ± 0.20
$\phi_n^{MCNP} + \sigma\left(\phi_n^{MCNP}\right)$	-0.89 ± 0.16	-1.92 ± 0.15	-16.2 ± 0.3	-17.0 ± 0.3	-8.95 ± 0.21	-7.55 ± 0.25	+21.2 ± 0.4	-3.88 ± 0.20

As a consequence of the slight overall photon flux underestimation, the total photon power of 5.41 MW is mispredicted by about -4%. Photon power in the high-power section of the blanket is underestimated by 5 to 10%.

From these results, it can be concluded that the procedure currently in use at ANL for computing EBR-II broad-group photon-production matrices is satisfactory since it gives reasonably accurate photon power predictions when a good neutron flux estimate is available. However, even if an error-free broad-group neutron flux is available, photon power underpredictions of 5 to 15% in reflector regions, and of 4 to 8% in the blanket, should be expected. The use of improved neutron spectra for collapsing the intermediate-group matrices in those regions would reduce these errors.

VI. CONCLUSION

Recent progress in the development EBR-II analysis methods have made it theoretically possible to obtain more accurate predictions of important operational variables such as criticality and neutron/photon

flux and power distributions, in spite of the difficulties arising from the unique characteristics of the reactor. Numerical tests have shown that the VARIANT nodal code yields eigenvalue and power predictions as accurate as finite difference and S_n codes, at a small fraction of the cost. On the other hand, detailed comparisons with continuous-energy Monte Carlo results have confirmed that the use of the diffusion-theory approximation for computing neutron regional collapsing spectra introduces significant errors in reflector and blanket broad-group cross sections, kerma factors, and photon-production matrices. Nonetheless, the impact of these errors on the EBR-II neutron/photon power distributions were found to be acceptably small, except possibly in the blanket region. Separate numerical tests have shown that the photon group structure, cross sections, and kerma factors are all satisfactory, giving photon power predictions that are in very good agreement with continuous-energy Monte Carlo results.

REFERENCES

1. H. HENRYSON II, B. J. TOPPEL, and C. G. STENBERG, "MC2-2: A Code to Calculate Fast Neutron Spectra and Multigroup Cross Sections," ANL-8144, Argonne National Laboratory (June 1976).

2. B. J. TOPPEL, H. HENRYSON II, and C. J. STENBERG, "ETOE-2/MC2-2/SDX Multigroup Cross Section Processing," RSIC Seminar on Multigroups Cross Section, Oak Ridge (March 14, 1978).

3. R. N. HILL, T. H. FANNING, and P. J. FINCK, "An Evaluation of Multigroup Flux Predictions in the EBR-II Core," Proc. Top. Mtg. Advances in Reactor Physics, Charleston, South Carolina (March 1992).

4. C. B. CARRICO, E. E. LEWIS, and G. PALMIOTTI, "Three-Dimensional Variational Nodal Transport Methods for Cartesian, Triangular, and Hexagonal Criticality Calculations," Nucl. Sci. Eng., 111, 168 (1992).

5. G. PALMIOTTI, C. B. CARRICO, and E. E. LEWIS, "Variational Nodal Transport Methods with Anisotropic Scattering," Nucl. Sci. Eng., 115, 233 (1993).

6. K. L. DERSTINE, "DIF3D: A Code to Solve One-, Two-, and Three-Dimensional Finite Difference Diffusion Theory Problems," ANL-82-64, Argonne National Laboratory (1984).

7. W. F. WALTERS et al., "TWOHEX: A Code Package for Two-Dimensional, Neutral-Particle Transport in Equilateral Triangular Meshes," Proc. Int. Mtg. Advances in Nuclear Engineering Computational Methods, Knoxville, Tennessee, 1, 64 (April 1985).

8. R. D. LAWRENCE, "The DIF3D Nodal Neutronics Option for Two- and Three-Dimensional Diffusion Theory Calculations in Hexagonal Geometry," ANL-83-1, Argonne National Laboratory (March 1983).

9. J. R. LIAW and P. J. FINCK, "Monte-Carlo-Based Validation of Neutronic Methodology for EBR-II Analyses," Trans. Am. Nucl. Soc., 68, 434 (1993).

10. J. F. BRIESMEISTER, Editor, "MCNP - A General Monte Carlo Code for Neutron and Photon Transport," Version 3A, LA-7396-M, Rev. 2, Los Alamos National Laboratory (September 1986).

11. R. E. ALCOUFFE et al., "User's Guide for TWODANT: A Code Package for Two-Dimensional, Diffusion-Accelerated, Neutral-Particle Transport," LA-10049-M, Los Alamos National Laboratory, (February 1990).